Journal of
Mechanics of
Materials and Structures

EXACT SOLUTIONS OF AFM SCANNING PROBES SUBJECTED TO TIP-SAMPLE FORCES

Shueei-Muh Lin, Sen-Yung Lee and Kuen-Wey Lin

EXACT SOLUTIONS OF AFM SCANNING PROBES SUBJECTED TO TIP-SAMPLE FORCES

SHUEEI-MUH LIN, SEN-YUNG LEE AND KUEN-WEY LIN

In this study, an analytical method for the static deflection of an AFM nonuniform probe subjected to tip-sample forces is presented. The effects of the Lennard-Jones and electrostatic noncontact forces and a contact force on the deflection of a cantilever are investigated. The contact force is simulated by the Derjaguin–Muller–Toporov model. In general, when an atomic force microscopy is used to measure a sample's topography and properties, a jump phenomenon of a cantilever usually exists. Unfortunately, there is a lack of a complete and precise description about this jump phenomenon. This proposed analytical method is helpful to investigate precisely the jump phenomenon. Moreover, the effects of several parameters on the jump phenomenon are studied. Finally, several simple and general relations between the deflection of beam and the tip-sample distance are presented.

1. Introduction

Atomic force microscopy (AFM) force-distance curves have become a fundamental tool in several fields in research, such as surface science, material engineering, biochemistry and biology [Cappella and Dietler 1999]. Nanoscale wires are usually coated on a substrate as a semiconductor. The materials of wire and substrate are different. Therefore, the contact potential differences between the tip and a sample's surfaces are also different. Because of it, an electrostatic force exists between the tip and the sample's surface, which will result in error when measuring a sample's topography. Kelvin probe force microscopy (KPFM) is a powerful measuring technique on a nanometer scale; it uses an atomic force microscopy with an electrostatic force. It is currently used to image proteins [Rossell et al. 2003] and the contact potential difference on a large variety of samples, such as semiconductors [Shikler et al. 1999; Katano et al. 2002]. The electrostatic force in a Kelvin probe force microscopy results commonly from the tip-sample potential difference and a compensated voltage between tip and sample. Sadewasser et al. [2003; 2004] investigated the resolution of KPFM and the influence of uncompensated electrostatic force on a sample's surface height measurements. They found that the accuracy of the measured step height was strongly dependent on the compensated d.c. voltage between tip and sample.

Several authors have investigated the electrostatic force between a tip and a sample's surface. Belaidi et al. [1997] calculated the electrostatic force acting on the tip of AFM by using the model of equivalent charge distribution. They compared the equivalent charge model with several analytical models simulating the electrostatic forces. They recommended the use of two approximate models for the tip-plane interaction: the spherical model for small and large distance and the perfect cone model or uniformly

---

charged line for intermediate distances. Further, Belaidi et al. [1998] used the finite element method to simulate the electrostatic force between two conducting parts placed at different voltages. Law and Rieutord [2002] investigated various electrostatic models describing the relation between a polarized atomic force microscopy tip and a sample. They found that the model by Hudlet et al. [1998] provided an excellent description of the experimental data. In our study this model is used to investigate the response of an AFM beam subjected to an electrostatic force.

When the tip-sample distance is in the order of interatomic spacing, chemical bonding can occur. This bond is usually modeled by a phenomenological Lennard-Jones potential. The corresponding Lennard-Jones force is composed of a repulsive force and a van der Waals force. It is a noncontact force. If the tip penetrates a sample's surface, a contact force occurs. When the cantilever approaches the surface, the cantilever becomes unstable and jumps onto a sample's surface. It is referred to as the jump-to-contact discontinuity. When the cantilever retracts from a sample's surface, a jump phenomenon happens also. That's referred to as the jump-off-contact discontinuity. The difference in path between approach and withdrawal curves is usually called *force-displacement curve hysteresis*. Theoretically, the necessary condition of the jump phenomenon is that the tip-sample force gradient is larger than the effective elastic constant of a cantilever. Unfortunately, no complete mathematical theorem of the system has ever been derived. Obviously, a rigorous theorem is needed to investigate the jump phenomenon. Moreover, the corresponding analytical solutions can help to determine the functional relationships between operational parameters and the physical tip-sample force.

So far, due to the complexity no analytical solution for the response of a nonuniform probe subjected to the Lennard-Jones and electrostatic noncontact forces and a contact force exists. Moreover, the jump phenomenon in measurement of a general system has not been investigated yet. In this study, the exact solution of an AFM nonuniform probe subjected to noncontact and contact forces is derived. Moreover, we investigate the jump phenomenon in measurement of a general system.

2. Governing equation and boundary conditions

The static response of a nonuniform probe with elastic root, subjected to the weights of beam and the non-contact Lennard-Jones and electrostatic forces and a contact force is investigated, as shown in Figure 1. Generally, the length and thickness of an AFM beam are approximately 100 and 2 μm, respectively. The deformation is less than approximately 100 nm. Therefore, the Bernoulli–Euler theory is suitable for the AFM probe.

In this study, the following dimensionless quantities are considered:

$$b(\xi) = \frac{E(x)I(x)}{E(0)I(0)}, \qquad c_{v1} = \frac{H_1 R L^3}{E(0)I(0)L_c^9}, \qquad c_{v2} = \frac{H_2 R L^3}{E(0)I(0)L_c^3}, \qquad c_e = \frac{\pi \varepsilon_0 (V - V_0)^2 L^3}{E I L_c},$$

$$\bar{D}_0 = \frac{D_0}{L_c}, \quad f_b = \frac{m_t g L^3}{E(0)I(0)L_c}, \quad f_c = \bar{k}_{\text{eff}} \bar{R}^{1/2} \bar{D}^{3/2} - 2\pi \bar{S}_e \bar{R}, \quad f_l = \frac{c_{v1}}{180(\bar{D}_0 - w)^8} - \frac{c_{v2}}{6(\bar{D}_0 - w)^2},$$

$$f_e = c_e \bar{F}, \quad \bar{k}_{\text{eff}} = \frac{4}{3\pi^2} \frac{L^3 L_c}{I(0)} \left[\frac{1-v_t^2}{E_t/E_t(0)} + \frac{1-v_s^2}{E_s/E_t(0)} \right]^{-1}, \quad p(\xi) = \frac{P(x)L^4}{E(0)I(0)L_c}, \quad \bar{R} = \frac{R}{L_c},$$

$$\bar{S}_e = \frac{S_e L^3 L_c}{EI}, \quad w(\xi) = \frac{W(x)}{L_c}, \quad \beta_1 = \frac{K_\theta L}{E(0)I(0)}, \quad \beta_2 = \frac{K_T L^3}{E(0)I(0)},$$

$$\gamma_{11} = \frac{\beta_1}{1+\beta_1}, \quad \gamma_{12} = \frac{1}{1+\beta_1}, \quad \gamma_{21} = \frac{\beta_2}{1+\beta_2}, \quad \gamma_{22} = \frac{1}{1+\beta_2}, \quad \xi = \frac{x}{L},$$

where A is the cross sectional area, D_0 the initial distance between the tip and the sample without deformation, E the Young's modulus, f_b the dimensionless tip weight, f_e the dimensionless interacting force, g the gravity acceleration, I the area moment of inertia, K_T the translational spring constant at the left end, K_θ the rotational spring constants, L the length of beam, L_c the characteristic length, m_t the tip mass, P the beam weight per unit length, W the flexural displacement, x the coordinate along the beam, ρ the mass density per unit volume. Because the length of beam is more than $10\,\mu$m and the deformation of a cantilever is less than 20 nm, their scale orders are greatly different. For the dimensionless expression of deformation and avoiding the numerical transaction error, one introduces a characteristic length L_c, which is in the scale order as that of deformation, for example, $L_c = 10$ nm.

In terms of the above dimensionless quantities, the governing differential equation of the Euler–Bernoulli beam subjected to its weight $p(\xi)$ is

$$\frac{d^2}{d\xi^2} \left[b(\xi) \frac{d^2 w}{d\xi^2} \right] = p(\xi). \tag{1}$$

The boundary conditions of an elastic root of beam at $\xi = 0$ are expressed as

$$\gamma_{12} \frac{d^2 w}{d\xi^2} - \gamma_{11} \frac{dw}{d\xi} = 0, \quad \gamma_{22} \frac{d}{d\xi} \left[b(\xi) \frac{d^2 w}{d\xi^2} \right] + \gamma_{21} w = 0. \tag{2}$$
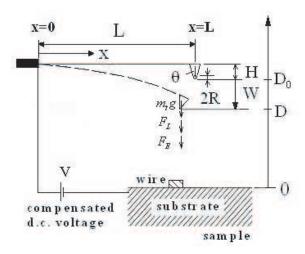

Figure 1. Geometry and coordinate system of a microprobe.

There are a number of forces acting at the tip: the tip weight, the Lennard-Jones force and the electrostatic force. However, no moment acts at the tip of a beam. Boundary conditions at $\xi = 1$ are expressed as

$$\frac{d^2w}{d\xi^2} = 0, \qquad \frac{d}{d\xi}\left[b(\xi)\frac{d^2w}{d\xi^2}\right] = -f_b + f_{ts}, \tag{3}$$

where f_{ts} is the dimensionless tip-sample interacting force. The noncontact force between the tip and the sample by a combination of a longrange electrostatic force f_e and a shortrange (Lennard-Jones) force f_l. The contact force f_c is usually described by macroscopic continuum theories using Derjaguin–Muller–Toporov (DMT) model [Hudlet et al. 1998]. The tip-sample force is composed of the noncontact and contact forces and can be expressed as

$$f_{ts} = \begin{cases} f_l + f_e, & D > D_c, \\ f_c, & D < D_c, \end{cases} \tag{4}$$

where D_c is the point of contact [Hölscher 2003]. These forces are described below.

It is well known that when the tip-sample distance is decreased to the nanometer scale, a longrange attractive force between a tip and a sample exits. When the tip-sample distance is further decreased, a shortrange repulsive force exits. These forces are usually modeled by a phenomenological Lennard-Jones force which is composed of a repulsive force and a van der Waals force. The Lennard-Jones force F_L is [Belaidi et al. 1998]

$$F_L = \frac{H_1 R}{180 D^8} - \frac{H_2 R}{6 D^2},$$

where the first term on the righthand side is a repulsive force and the second term is the van der Waals force, H_i the Hamaker constant, D the tip-sample distance, R the tip radius.

In addition to the van der Waals attractive force, there may be an electrostatic force due to a potential difference between the working functions of a tip and a sample. If the sample is made of only one material, it is possible to measure the sample's topography correctly. But if nanoscale wires are coated on a substrate, the materials of the wire and the substrate are different. Therefore, the contact potential differences V_0 between the tip and wires are also different from that between the tip and the substrate. These electrostatic forces will induce different deformations of a cantilever. Neglecting the effects of these electrostatic forces will results in an error when measuring a sample's topography. In order to get an accurate topography of the sample, one usually applies a d.c. voltage V between the tip and a sample's surface to compensate for the contact potential difference. If $V = V_0$, one obtains accurate topography of the sample. The electrostatic force F_E can be expressed as [Law and Rieutord 2002]

$$F_E = \pi \varepsilon_0 (V - V_0)^2 \bar{F}(D),$$

where the parameter $\bar{F}(D)$ depends on the geometry of a tip. In this study, we consider the model by Hudlet et al. [1998]. The parameter $\bar{F}(D)$ for a tip as a spherical apex and cone is expressed as

$$\bar{F}(D) = -K^2\left[\ln\left(\frac{H}{D + R(1 - \sin\theta)}\right) - 1 + \frac{R\cos^2\theta / \sin\theta}{D + R(1 - \sin\theta)}\right] - \frac{R^2(1 - \sin\theta)}{D[D + R(1 - \sin\theta)]},$$

where H is the height of tip and $K = 1/\ln(\tan(\theta/2))$.

The static tip-sample interactions are usually described by macroscopic continuum theories such as Hertzian, Johnson–Kendall–Roberts (JKR) and Derjaguin–Muller–Toporov (DMT) contact models [Hölscher 2003]. In this study, we consider the DMT model. Note that the other models can be easily solved by using the proposed method. The tip-sample interaction in the DMT model is

$$F_c = k_{\mathrm{eff}} R^{1/2} |D|^{3/2} - 2\pi S_e R,$$

where S_e is the surface energy and $k_{\mathrm{eff}} = 4[(1 - v_s^2)/E_s + (1 - v_t^2)/E_t]^{-1}/3\pi^2$ in which $\{v_s, E_s\}$ and $\{v_t, E_t\}$ are the Poisson ratios and Young's modulus of sample and tip, respectively.

3. Solution method

In general, it is difficult to derive the analytical solution of a system with nonlinear boundary conditions. Nevertheless, the following method is proposed to derive its exact solution. First, one chooses a relation among the displacement w and two new variables s and v. Upon substituting the relation into the original nonlinear system, the original system will be transformed into two linear independent subsystems in terms of s and v. The solutions s and v of the two linear subsystems can be easily derived. Finally, substituting these solutions back into the relation and letting the relation in Equation (5) satisfy the tip displacement condition, one obtains the general solution. It should be noted that the tip displacement condition is an implicit function. However, one can easily determine its solution by numerical methods.

3.1. *Change of variable.* The relation among the displacement w and two new variables s and v is chosen as [Lee and Lin 1996]

$$w(\xi) = v(\xi) - (f_b - f_{ts})s(\xi), \tag{5}$$

where $s(\xi)$ is a shifting function, chosen to satisfy the following differential equation

$$\frac{d^2}{d\xi^2}\left[b(\xi)\frac{d^2 s}{d\xi^2}\right] = 0 \tag{6}$$

subject to boundary conditions

$$\gamma_{12}\frac{d^2 s}{d\xi^2} - \gamma_{11}\frac{ds}{d\xi} = 0, \qquad \gamma_{22}\frac{d}{d\xi}\left[b(\xi)\frac{d^2 s}{d\xi^2}\right] + \gamma_{21}s = 0, \quad \text{at} \quad \xi = 0, \tag{7}$$

$$\frac{d^2 s}{d\xi^2} = 0, \qquad\qquad \frac{d}{d\xi}\left[b(\xi)\frac{d^2 s}{d\xi^2}\right] = 1, \quad \text{at} \quad \xi = 1. \tag{8}$$

After substituting Equations (5)–(8) into Equations (1)–(4), one obtains differential equations in terms of $v(\xi, \tau)$. The transformed governing equation is

$$\frac{d^2}{d\xi^2}\left[b(\xi)\frac{d^2 v}{d\xi^2}\right] = p(\xi), \tag{9}$$

and the associated homogeneous boundary conditions are

$$\gamma_{12}\frac{d^2v}{d\xi^2} - \gamma_{11}\frac{dv}{d\xi} = 0, \qquad \gamma_{22}\frac{d}{d\xi}\left[b(\xi)\frac{d^2v}{d\xi^2}\right] + \gamma_{21}v = 0, \quad \text{at} \quad \xi = 0, \tag{10}$$

$$\frac{d^2v}{d\xi^2} = 0, \qquad\qquad \frac{d}{d\xi}\left[b(\xi)\frac{d^2v}{d\xi^2}\right] = 0, \quad \text{at} \quad \xi = 1. \tag{11}$$

The corresponding exact solutions $v(\xi)$ and $s(\xi)$ are to be derived in the following sections. Substituting these solutions into Equation (5), the general solution $w(\xi)$ is obtained. It should be noted that f_l and f_e are the function of the tip deflection $w(1)$. In other words, Equation (5) is an implicit function. However, it is very easy to determine the exact solution $w(\xi)$ of Equation (5) by numerical methods [Lin 1999].

3.2. Shifting functions. The shifting function $s(\xi)$ of Equation (6) can be written as

$$\frac{d}{d\xi}\left[b(\xi)\frac{d^2s}{d\xi^2}\right] = c_1 \quad \Rightarrow \quad b\frac{d^2s}{d\xi^2} = c_1\xi + c_2 \quad \Rightarrow \quad \frac{ds}{d\xi} = \int \frac{c_1\xi + c_2}{b(\xi)}d\xi + c_3,$$

$$\Rightarrow \quad s = \iint \frac{c_1\xi + c_2}{b(\xi)}d\xi + c_3\xi + c_4. \tag{12}$$

Substituting Equation (12) into the boundary conditions (7) and (8), one obtains the constants c_i as well as the shifting function

$$s(\xi) = \iint \frac{\xi - 1}{b(\xi)}d\xi - \frac{1}{\gamma_{11}}\left(\gamma_{12} + \gamma_{11}\int \frac{\xi - 1}{b(\xi)}d\xi\right)_{\xi=0}\xi - \frac{1}{\gamma_{21}}\left(\gamma_{22} + \gamma_{21}\iint \frac{\xi - 1}{b(\xi)}d\xi\right)_{\xi=0}.$$

If the cross section of beam is uniform, the dimensionless bending rigidity $b = 1$ and $s(\xi)$ becomes

$$s(\xi) = \tfrac{1}{6}\xi^3 - \tfrac{1}{2}\xi^2 - \frac{\gamma_{12}}{\gamma_{11}}\xi - \frac{\gamma_{22}}{\gamma_{21}}.$$

Further, if a uniform cantilever is considered, the shifting function becomes $s(\xi) = \tfrac{1}{6}\xi^3 - \tfrac{1}{2}\xi^2$, that is the same as that given by Lee and Lin [1996].

3.3. Transformed solution. The transformed solution $v(\xi)$ of Equations (9)–(11) can be written as

$$v(\xi) = V_p(\xi) + \sum_{i=1}^{4} D_i V_i(\xi), \tag{13}$$

where $V_p(\xi)$ is the particular solution. D_i is the constant to be determined. $V_i(\xi)$ are the four linearly independent fundamental solutions of Equation (9), which satisfy the following normalized condition

$$\begin{bmatrix} V_1(0) & V_2(0) & V_3(0) & V_4(0) \\ V_1'(0) & V_2'(0) & V_3'(0) & V_4'(0) \\ V_1''(0) & V_2''(0) & V_3''(0) & V_4''(0) \\ V_1'''(0) & V_2'''(0) & V_3'''(0) & V_4'''(0) \end{bmatrix} = \begin{bmatrix} 1 & 0 & 0 & 0 \\ 0 & 1 & 0 & 0 \\ 0 & 0 & 1 & 0 \\ 0 & 0 & 0 & 1 \end{bmatrix}. \tag{14}$$

The particular solution V_p and the fundamental solutions V_i can be derived easily by using the method proposed by Lee and Lin [1996].

Note that the proposed method can be used to solve the static measurement problem of a probe with arbitrary cross section and made of any material. It is well known that a conventional probe has a uniform or V-type cross-section. In the following sections we derive the analytical solutions for these conventional probes.

4. *V*-typed beam

The material properties and the height of the beam are assumed to be constant, while the width of the beam varies linearly with the taper ratio λ. If the taper ratio is negative, the geometry of the probe is V-typed. Consequently, the dimensionless bending rigidity $b = (1 + \lambda \xi)$ and the dimensionless body force $p = p_0(1 + \lambda \xi)$ where $p_0 = \rho A_0 g L^4/[E(0)I(0)L_c]$. Therefore, the transformed governing differential Equation (9) becomes

$$\frac{d^2}{d\xi^2}\left((1 + \lambda \xi)\frac{d^2 v}{d\xi^2}\right) = p_0(1 + \lambda \xi). \tag{15}$$

The particular solution of Equation (15) is easily obtained as

$$V_p = \frac{p_0}{18\lambda}\xi^3 + \frac{p_0}{72}\xi^4.$$

Obviously, the homogeneous differential Equation (15) can be expressed as

$$(1 + \lambda \xi)\frac{d^4 v}{d\xi^4} + 2\lambda \frac{d^3 v}{d\xi^3} = 0. \tag{16}$$

The four normalized fundamental solutions of Equation (16) are:

$$V_1(\xi) = 1, \qquad V_2(\xi) = \xi, \qquad V_3(\xi) = \tfrac{1}{2}\xi^2, \qquad V_4(\xi) = \frac{\xi}{\lambda^2} + \frac{\xi^2}{2\lambda} - \frac{1 + \lambda \xi}{\lambda^3}\ln(1 + \lambda \xi). \tag{17}$$

These fundamental solutions in Equation (17) satisfy the normalized condition in Equation (14). If $\lambda = 0$, the corresponding fourth fundamental solution $V_4(\xi) = \xi^3/6$.

Upon substituting the solutions (13) and (17) into the boundary conditions (10) and (11), the coefficients D_j are derived

$$D_1 = \frac{-\gamma_{22}p_0(\lambda^2 + 5\lambda - 6)}{6\gamma_{21}}, \quad D_2 = \frac{\gamma_{12}p_0(3\lambda + 1)}{6\gamma_{11}}, \quad D_3 = \frac{p_0(3\lambda + 1)}{6}, \quad D_4 = \frac{-p_0(1 + \lambda)^3}{3\lambda}.$$

Meanwhile, the shifting function is

$$s = \frac{1}{2\lambda}\xi^2 - \left(1 + \frac{1}{\lambda}\right)\frac{(1 + \lambda \xi)}{\lambda^2}[\ln(1 + \lambda \xi) - 1] - \frac{\gamma_{12}}{\gamma_{11}}\xi - \frac{\gamma_{22}}{\gamma_{21}} - \left(1 + \frac{1}{\lambda}\right)\frac{1}{\lambda^2}. \tag{18}$$

Substituting the solutions (17) and (18) into the relation (5) and letting $\xi = 1$, the solution of tip deflection becomes

$$w(1) = p_0 \bar{V}_1 - (f_b - f_{ts})s(1), \tag{19}$$

where

$$\bar{V}_1 = \frac{1}{18\lambda} + \frac{1}{72} - \frac{\gamma_{22}}{6\gamma_{21}}(\lambda^2 + 5\lambda - 6) + \frac{(3\lambda+1)}{6}\left(\frac{\gamma_{12}}{\gamma_{11}} + \frac{1}{2}\right) - \frac{(1+\lambda)^3}{3\lambda}\left(\frac{1}{\lambda^2} + \frac{1}{2\lambda} - \frac{1+\lambda}{\lambda^3}\ln(1+\lambda)\right),$$

$$s(1) = \frac{1}{2\lambda} - \left(1 + \frac{1}{\lambda}\right)\frac{(1+\lambda)}{\lambda^2}[\ln(1+\lambda) - 1] - \frac{\gamma_{12}}{\gamma_{11}} - \frac{\gamma_{22}}{\gamma_{21}} - \left(1 + \frac{1}{\lambda}\right)\frac{1}{\lambda^2}.$$

Because the force f_{ts} depends on the tip deflection $w(1)$, Equation (19) is an implicit function. Using the numerical method proposed by [Lin 1999], the exact solution $w(1)$ of Equation (19) can be easily determined.

If consider only the van der Waals force, Equation (19) is reduced to be

$$r^3 - 2dr^2 + d^2r + \tfrac{1}{6}c_{v2}s(1) = 0,$$

where the dimensionless undeformed tip-sample distance $d = \bar{D}_0 - w_s$ and deformed distance $r = w(1) - w_s$. Here w_s denotes the tip deflection due to the weight of probe $w_s = p_0\bar{V}_1 - f_b s(1)$. One can also derive another relation given by

$$d = \sqrt{\frac{-c_{v2}s(1)}{6r}} + r. \tag{20}$$

It tell us that the deformed tip-sample distance can be directly predicted via the relation (20). Moreover, the sensitivity of measurement depends on the dimensionless coefficient c_{v2} and the shifting function $s(1)$. When r is large, d approaches r. When r is very small, d will be very large.

5. Uniform beam

For a uniform beam the bending rigidity $b = 1$ and the taper ratio $\lambda = 0$. The governing differential Equation (15) becomes

$$\frac{d^4v}{d\xi^4} = p. \tag{21}$$

The four normalized fundamental solutions and the particular solution of Equation (21) are

$$V_1(\xi) = 1, \qquad V_2(\xi) = \xi, \qquad V_3(\xi) = \tfrac{1}{2}\xi^2, \qquad V_4(\xi) = \tfrac{1}{6}\xi^3, \qquad V_p = \frac{p}{24}\xi^4.$$

The transformed solution v and the shifting function s are, respectively,

$$v(\xi) = p\left(\frac{\gamma_{22}}{\gamma_{21}} + \frac{\gamma_{12}}{2\gamma_{11}}\xi + \tfrac{1}{4}\xi^2 - \tfrac{1}{6}\xi^3 + \tfrac{1}{24}\xi^4\right), \qquad s(\xi) = \left(\tfrac{1}{6}\xi^3 - \tfrac{1}{2}\xi^2 - \frac{\gamma_{12}}{\gamma_{11}}\xi - \frac{\gamma_{22}}{\gamma_{21}}\right). \tag{22}$$

Substituting Equation (22) into the relation (5), one obtains the deflection of beam

$$w(\xi) = p\left(\frac{\gamma_{22}}{\gamma_{21}} + \frac{\gamma_{12}}{2\gamma_{11}}\xi + \tfrac{1}{4}\xi^2 - \tfrac{1}{6}\xi^3 + \tfrac{1}{24}\xi^4\right) - (f_b - f_{ts})\left(\tfrac{1}{6}\xi^3 - \tfrac{1}{2}\xi^2 - \frac{\gamma_{12}}{\gamma_{11}}\xi - \frac{\gamma_{22}}{\gamma_{21}}\right).$$

The corresponding tip deflection due to the beam weight is found as

$$w_s = p\left(\frac{\gamma_{22}}{\gamma_{21}} + \frac{\gamma_{12}}{2\gamma_{11}} + \tfrac{1}{8}\right) + f_b\left(\tfrac{1}{3} + \frac{\gamma_{12}}{\gamma_{11}} + \frac{\gamma_{22}}{\gamma_{21}}\right).$$
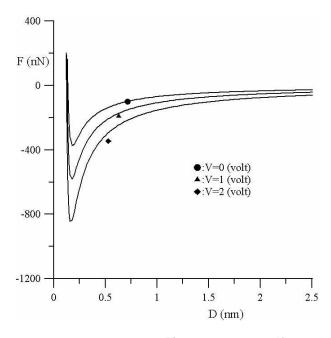
Figure 2. Force-distance curve ($H_1 = 10^{-76}$ Joule, $H_2 = 10^{-19}$ Joule, $H = 6\,\mu$m, $R = 150$ nm, $\theta = 12^0$, $V_0 = 0$).

Further, if we apply only the van der Waals force to a uniform beam, the relation (20) becomes

$$d = \sqrt{\frac{c_{v2}\left(\frac{1}{3} + \frac{\gamma_{12}}{\gamma_{11}} + \frac{\gamma_{22}}{\gamma_{21}}\right)}{6r}} + r.$$

6. Numerical results and discussion

In this section we investigate the effects of the parameters on the deflection of a probe. Figure 2 shows the relation between the interacting force and the tip-sample distance. A probe is considered to be subjected to both the Lennard-Jones and electrostatic noncontact interacting forces. The influence of the d.c. voltage V on the interacting tip-sample force is presented. For large distances ($D > 2$ nm), these two kinds of forces are small. Decreasing the distance dramatically increases the attractive force especially under a larger d.c. voltage V. When the tip-sample distance is very small, the repulsive force becomes dominant.

Figure 3 shows the relation between the undeformed tip-sample distance D_0 and the deformed distance D. If the tip is far from the sample, the attractive force to the probe is small and the deflection of the probe is small. Therefore, the tip-sample distance D is large. In other words, the larger D_0 is, the larger D is. It is shown in Figure 3 that when D_0 is large, the relation between D_0 and D is one-to-one. In other words, there is only one root D of Equation (19) in the domain $D_0 > D_{c2}$. If $D_{c1} < D_0 < D_{c2}$, there are three roots $\{D_1, D_2, D_3\}$ of Equation (19) in this domain. If $D_0 < D_{c1}$, there is only one root D of Equation (19). What it means is that when the probe reaches the sample at a distance approaching the critical distance D_{c2}, the jump-to-contact phenomenon will occur. On the other hand when the probe is
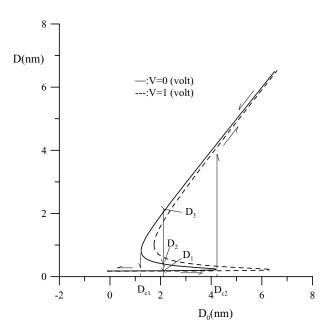
Figure 3. The relation between the undeformed distance and the tip-sample distance ($b = 45\,\mu\text{m}$, $h = 4.5\,\mu\text{m}$, $L = 200\,\mu\text{m}$, $L_c = 10\,\text{nm}$, $E = 70.3 \times 10^9\,\text{Pa}$, $H_1 = 10^{-76}\,\text{Joule}$, $H_2 = 10^{-19}\,\text{Joule}$, $H = 6\,\mu\text{m}$, $p = 0$, $R = 150\,\text{nm}$, $\rho = 2.5 \times 10^3\,\text{kg/m}^3$, $\theta = 12^0$, $V_0 = 0$).
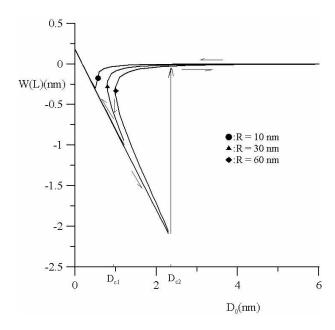

Figure 4. The influence of the radius of tip on the deflection of probe ($b = 45\,\mu\text{m}$, $h = 3.5\,\mu\text{m}$, $L = 170\,\mu\text{m}$, $L_c = 10\,\text{nm}$, $E = 70.3 \times 10^9\,\text{Pa}$, $H_1 = 10^{-76}\,\text{Joule}$, $H_2 = 10^{-19}\,\text{Joule}$, $H = 6\,\mu\text{m}$, $p = 0$, $\rho = 2.5 \times 10^3\,\text{kg/m}^3$, $\theta = 12^0$, $V = V_0 = 0$).
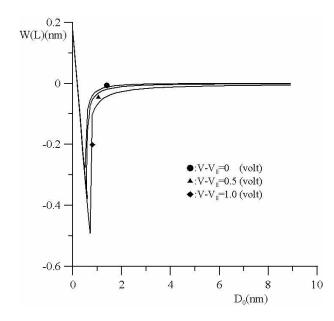
Figure 5. The influence of the d.c. voltage on the deflection of probe ($b = 45 \, \mu$m, $h = 4.5 \, \mu$m, $L = 170 \, \mu$m, $L_c = 10$ nm, $E = 70.3 \times 10^9$ Pa, $H_1 = 10^{-76}$ Joule, $H_2 = 10^{-19}$ Joule, $H = 6 \, \mu$m, $p = 0$, $R = 20$ nm, $\rho = 2.5 \times 10^3$ kg/m^3, $\theta = 12^0$, $V_0 = 0$).

pulled off to the critical distance D_{c1}, the jump-off-contact phenomenon will also occur. In other words, if D_0 is in the domain $[D_{c1}, D_{c2}]$, the jump phenomenon will happen. Moreover, one sees from Figure 3 that increasing the contact potential difference $(V - V_0)$ increases the domain $[D_{c1}, D_{c2}]$.

Figure 4 shows the influence of the radius of tip on the deflection. It is observed from the case with $R = 60$ nm that when the probe approaches a sample's surface, the attractive tip-sample force pulls the probe down gradually. If the undeformed tip-sample distance D_0 is decreased to the critical value D_{c2}, the jump-to-contact phenomenon occurs. The probe will be pulled down instantly. When the undeformed distance D_0 is decreased further, the repulsive tip-sample force pushes the probe up. The tip deflection of the probe is decreased. When the probe is pulled away from a sample to the critical value D_{c1}, the jump-off-contact phenomenon occurs. The probe will be pulled up instantly. We learn from Figure 4 that increasing the radius of tip R increases the jump domain $[D_{c1}, D_{c2}]$. Moreover, when the radius of tip is decreased to 10 nm, the jump phenomenon disappears.

Figure 5 shows the influence of the contact potential difference $(V - V_0)$ on the jump phenomenon and the tip deflection. We find that increasing the contact potential difference enhances the jump phenomenon. Figure 6 shows the influence of the elastic constant k of a probe on the jump phenomenon and the tip deflection. We learn that given $k = 4.612$ N/m, the jump phenomenon happens with the jump domain $[D_{c1}, D_{c2}]$. Moreover, increasing the elastic constant k will decrease the jump domain. When the elastic constant k is increased over a critical value, the jump phenomenon disappears. Finally, the effect of a contact force simulated in the DTM model on the tip deflection is investigated. Figure 7 shows the relation among the radius of tip and the tip deflection and the penetrative distance denoted as $-D$. The
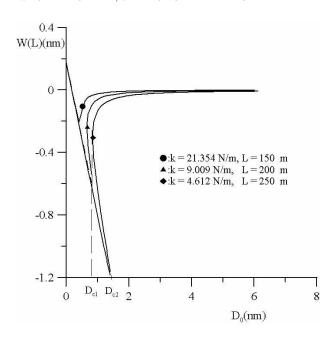
Figure 6. The influence of the elastic constant on the deflection of probe ($b = 45\,\mu$m, $h = 4.5\,\mu$m, $L_c = 10$ nm, $E = 70.3 \times 10^9$ Pa, $H_1 = 10^{-76}$ Joule, $H_2 = 10^{-19}$ Joule, $H = 6\,\mu$m, $p = 0$, $R = 20$ nm, $\rho = 2.5 \times 10^3$ kg/m^3, $\theta = 12^0$, $V = 0.5$ volt, $V_0 = 0$).
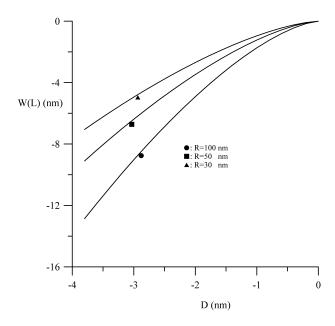

Figure 7. The relation among the penetrative distance, the radius of tip and the deflection of beam subjected to a contact force ($b = 45\,\mu$m, $D_c = 0.37$ nm, $h = 4.5\,\mu$m, $E_s = E_t = 70.3 \times 10^9$ Pa, $v_s = v_t = 0.2$, $H = 6\,\mu$m, $p = 0$, $S_e = 0$, $\rho = 2.5 \times 10^3$ kg/m^3, $\theta = 12^0$, $V = V_0 = 0$; $k = 9.009$ N/m, $L = 200\,\mu$m).

penetrative distance is a distance that the tip penetrates through a sample's surface. We observe that increasing the penetrative distance and the radius of tip increases the deflection of beam.

7. Conclusion

In this paper we study the static measurement of an AFM by using the Bernoulli–Euler beam theory. Its boundary conditions involve several nonlinear tip-sample noncontact and contact forces. The static analytical solution of a general system can be easily derived by the proposed method. We conclude that if only the van der Waals force is considered, the tip-sample distance d is proportional to the van der Waals coefficient c_{v2} and the shifting function $s(1)$. When the tip radius r is large, the magnitude of d is close to r. The effects of several parameters on the jump phenomenon are investigated. To sum up, we have discovered several trends as follows:

(1) increasing the radius of tip R increases the jump domain $[D_{c1}, D_{c2}]$. If the radius of tip is small enough, the jump phenomenon disappears;

(2) increasing the contact potential difference $(V - V_0)$ enhances the jump phenomenon;

(3) increasing the elastic constant k of a probe decreases the jump phenomenon.

References

[Belaidi et al. 1997] S. Belaidi, P. Girard, and G. Leveque, "Electrostatic forces acting on the tip in atomic force microscopy: modelization and comparison with analytic expressions", *J. Appl. Phys.* **81**:3 (1997), 1023–1030.

[Belaidi et al. 1998] S. Belaidi, F. Lebon, P. Girard, G. Leveque, and S. Pagano, "Finite element simulations of the resolution in electrostatic force microscopy", *Appl. Phys. A* **66**:supplement 1 (1998), s239–s243.

[Cappella and Dietler 1999] B. Cappella and G. Dietler, "Force-distance curves by atomic force microscopy", *Surf. Sci. Rep.* **34**:1-3 (1999), 1–104.

[Hölscher 2003] H. Hölscher, "Analysis of microscopy and spectroscopy experiments", pp. 349–369 in *Noncontact atomic force microscopy*, edited by S. Morita et al., Springer, 2003.

[Hudlet et al. 1998] S. Hudlet, M. Saint Jean, C. Guthmann, and J. Berger, "Evaluation of the capacitive force between an atomic force microscopy tip and a metallic surface", *Eur. Phys. J. B* **2** (1998), 5–10.

[Katano et al. 2002] Y. Katano, T. Doi, H. Ohno, and K. Yoh, "Surface potential analysis on doping superlattice by electrostatic force microscope", *Appl. Surf. Sci.* **188**:3-4 (2002), 399–402.

[Law and Rieutord 2002] B. M. Law and F. Rieutord, "Electrostatic forces in atomic force microscopy", *Phys. Rev. B* **66** (2002), #035402.

[Lee and Lin 1996] S. Y. Lee and S. M. Lin, "Dynamic analysis of non-uniform beams with time dependent elastic boundary conditions", *J. Appl. Mech.* (*Trans. ASME*) **63** (1996), 474–478.

[Lin 1999] S. M. Lin, "Dynamic analysis of rotating nonuniform Timoshenko beams with an elastically restrained root", *J. Appl. Mech.* (*Trans. ASME*) **66** (1999), 742–749.

[Rossell et al. 2003] J. P. Rossell, S. Allen, M. C. Davies, C. J. Roberts, S. J. B. Tendler, and P. M. Williams, "Electrostatic interactions observed when imaging proteins with the atomic force microscope", *Ultramicroscopy* **96**:1 (2003), 37–46.

[Sadewasser et al. 2003] S. Sadewasser, T. Glatzel, R. Shikler, Y. Rosenwaks, and M. C. Lux-Steiner, "Resolution of Kelvin probe force microscopy in ultrahigh vacuum: comparison of experiment and simulation", *Appl. Surf. Sci.* **210**:1-2 (2003), 32–36.

[Sadewasser et al. 2004] S. Sadewasser, P. Carl, T. Glatzel, and M. C. Lux-Steiner, "Influence of uncompensated electrostatic force on height measurements in non-contact atomic force microscopy", *Nanotechnology* **15**:2 (2004), s14–s18.

[Shikler et al. 1999] R. Shikler, T. Meoded, N. Fried, and Y. Rosenwaks, "Potential imaging of operating light-emitting devices using Kelvin force microscopy", *Appl. Phys. Lett.* **74**:20 (1999), 2972–2974.

SHUEEI-MUH LIN: smlin@mail.ksu.edu.tw
Mechanical Engineering Department, Kun Shan University, Tainan 710-03, Taiwan

SEN-YUNG LEE: sylee@mail.ncku.edu.tw
Mechanical Engineering Department, National Cheng Kung University, Tainan 701, Taiwan

KUEN-WEY LIN: evanlin@itri.org.tw
Mechanical Engineering Department, National Cheng Kung University, Tainan 701, Taiwan